Influence of lattice polarizability on interacting Li-induced dipoles distributed in incipient ferroelectric $KTaO_3$

Yuki Ichikawa and Koichiro Tanaka*
Department of Physics, Graduate School of Science, Kyoto University, Sakyo-ku, Kyoto 606-8502, Japan
(Received 15 March 2007; revised manuscript received 27 February 2008; published 2 April 2008)

Susceptibility purely originated from the Li-induced quasistatic dipoles in relaxor $K_{1-x}Li_xTaO_3$ has been extracted from low-frequency permittivity using terahertz time-domain spectroscopy. The temperature dependence of the extracted susceptibility has an anomaly at the critical temperature T_a near 100 K with the critical slowing down of the low-frequency relaxation process. From a detailed analysis of the extracted susceptibility, we attributed the main part of the susceptibility for $x \leq 0.036$ to the high-frequency relaxation process and concluded that there are two relevant interactions that govern the ferroelectric coupling between Li-induced dipoles and that the interplay of the two interactions gives rise to a complex temperature dependence of the susceptibility originated from Li-induced dipoles. Below the critical concentration $x < 0.022$, short-range interaction between individual Li ions should be dominant. Above the critical concentration, $x > 0.022$, Coulomb interaction should be dominant. The crossover from the low-temperature glasslike phase to the low-temperature ferroelectric domain-state across x_c in $K_{1-x}Li_xTaO_3$ is attributed to the interplay of the two kinds of interaction.

DOI: 10.1103/PhysRevB.77.144102 PACS number(s): 77.22.−d, 07.57.−c, 78.20.Ci, 78.30.−j

I. INTRODUCTION

A system in which impurity-induced dipoles are mediated in a highly polarizable lattice is one of the most attractive subjects in solid state physics because the combination of the dipoles and highly polarizable bulk phonon brings about novel critical phenomena.[1–4] $KTaO_3$ doped with lithium in a small concentration, $K_{1-x}Li_xTaO_3$ (KLT), is such a material, and it provides an ideal system for the subject. The pure $KTaO_3$ maintains an ABO_3 cubic Perovskite structure as low as the liquid-helium temperature without undergoing a ferroelectric phase transition (quantum paraelectricity).[5] The softening of the lowest transverse optical mode (TO_1 mode) is suppressed by the quantum effect. The impurity lithium ion replaces the potassium ion in the *A*-site of the host lattice. Because of the ion-radius misfit, small lithium ions take sextet-degenerate off-center positions along three equivalent ⟨100⟩ directions with a displacement as large as a quarter of the lattice constant.[6,7] The off-center displacements of lithium ions produce electric dipole moments, and the dipoles change their directions with the thermal hopping motions of lithium ions. The total relative complex dielectric constant in this system at frequency $\nu(\nu < 10$ THz) can be expressed as

$$\tilde{\epsilon}_r(\nu) = \tilde{\chi}_{\mathrm{Li}}(\nu) + \tilde{\chi}_{\mathrm{TO}_1}(\nu) + \tilde{\epsilon}_\infty, \quad (1)$$

where $\tilde{\chi}_{\mathrm{Li}}(\nu)$ and $\tilde{\chi}_{\mathrm{TO}_1}(\nu)$ are the susceptibilities of Li-induced dipoles and the lattice polarization due to the TO_1 mode, respectively. $\tilde{\epsilon}_\infty$ represents the contributions of other polarizations with higher energy than that of the TO_1 mode. In frequencies lower than the THz region, we can regard $\tilde{\epsilon}_\infty$ as a real constant.

KLT has been intensively investigated since Yacoby *et al.* discovered the off-center displacement of the impurity Li by their Raman-scattering experiment.[8,9] The orientational relaxation of quasistatic dipoles due to the off-center hopping motion of Li ions undergoes critical slowing down toward the dipole freezing temperature.[10–12] Figure 1 shows a broadband spectrum of the complex dielectric constant from 1 Hz to 10 THz in KLT crystal ($x=0.020$), just above the dipole freezing temperature.[10–12] The upper and lower panels are the real and imaginary parts of the complex dielectric constant, respectively. A relaxation Debye step below 1 MHz is evident, as is the oscillation resonance at 1 THz. The former, which corresponds to $\tilde{\chi}_{\mathrm{Li}}(\nu)$, is the orientational relaxation originated from Li-induced dipoles.[10–12] The latter, which corresponds to $\tilde{\chi}_{\mathrm{TO}_1}(\nu)$, is the dispersion of the TO_1 soft mode in the $KTaO_3$ host lattice, whose frequency decreases with decreasing temperature by the anharmonicity of lattice.[13,14] Below the dipole freezing temperature, Kleemann *et al.* proposed, using birefringence measurements, that the phase boundary between the low-temperature glasslike phase ($x < x_c$) and ferroelectric domain-state-like phase ($x > x_c$) exists at around $x_c \cong 0.022$.[15]

The macroscopic dielectric properties of KLT, such as the dielectric susceptibility and residual polarization, have been

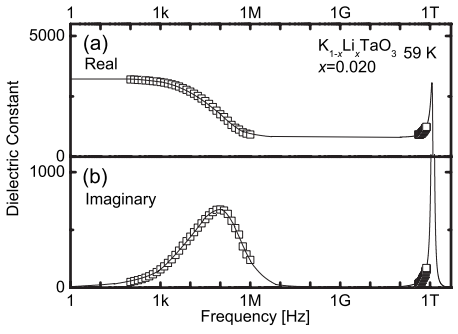

FIG. 1. Broadband dispersion of the complex dielectric constant in $K_{1-x}Li_xTaO_3$ ($x=0.020$) at 59 K, just above the dipole-freezing temperature. The dispersion from 100 Hz to 1 MHz is measured by measuring the ac impedance using an LCR meter. The dispersion in the THz region is determined by THz-TDS in this work. The solid curves are guides for the eye.

most intensively investigated since the 1970s.[1,2] Now, KLT is categorized as a relaxor material that shows a strongly frequency-dependent broad peak in the temperature dependence of the permittivity due to the critical slowing down of dipolar motion.[3,4,16] On the basis of rich experimental results regarding the dielectric properties, a number of theories on the diffused phase transition in KLT have been proposed.[17–22]

Much attention has also been directed to determining the correlation length of the Li-induced dipoles through various experiments, such as Raman scattering,[23] dielectric measurement,[24] second-harmonic generation,[25,26] x-ray diffuse scattering,[27] and neutron diffuse scattering.[28] The reported correlation lengths are summarized in Table II in the study by Yong *et al.*[28] Azzini *et al.* have also proposed the presence of two kinds of correlation: dipolar and quadrupolar.[25]

Raman scattering[29] and x-ray scattering[27] studies have revealed that the structural change takes place in KLT from cubic to tetragonal at the dipole freezing temperature. Neutron scattering[30] and hyper-Raman scattering[13,14,31] have also confirmed that the softening of the ferroelectric TO_1 mode is suppressed in KLT. These results are evidence of an order-disorder structural phase transition in KLT.

Terahertz time-domain spectroscopy (TDS)[32] established since 1983[33] by the development of ultrafast pulse laser techniques enabled to measure the dielectric constant in the THz region and to determine the soft-mode dispersion precisely.[34–41] Through the study of broadband dielectric measurements combined with the THz-TDS technique in KLT, it was confirmed that the dielectric contribution of the ferroelectric soft mode to the static dielectric constant in KLT showing the diffuse transition is relatively small and that the relaxation of Li-induced dipoles is the main contributor.[34–36]

Although a large number of experimental results have been presented and many theoretical models in which both the impurity dipoles and lattice are involved have been proposed, some important issues remain to be resolved regarding the two kinds of relaxators induced by the impurity Li ions,[12,20,36,42–49] namely, "$_{\pi/2}$ relaxation" with reorientation barrier height $U_{\pi/2} \sim 1000$ K and "π relaxation" with reorientation barrier height $U_{\pi} \sim 2500$ K; these two kinds are denoted as high-frequency (HF) relaxation process (RP) and low-frequency (LF) relaxation process (RP), respectively, in this paper. For example, one of the issues is regarding the origin of LF-RP, while that of HF-RP has been identified as the $_{\pi/2}$ flip of Li ions among the sextet-degenerate off-center positions.[20,36] Another issue, which we regard as the most important one, is that of the dominant interaction between the relaxational dipoles, which is considered to be in close relationship with the critical concentration x_c.[1,3,4,15,50]

The purpose of this study is to clarify the nature of the ordering from the viewpoint of the dominant interaction across x_c. For this purpose, we take a novel approach, that is, the extraction of the susceptibility due to the Li-induced dipoles $\tilde{\chi}_{\mathrm{Li}}(\nu)$ from $\tilde{\epsilon}_r(\nu)$ and the analysis combined with the temperature evolution of the host lattice polarizability. This treatment is justified by the fact that the time scales of $\tilde{\chi}_{\mathrm{Li}}(\nu)$ and $\tilde{\chi}_{\mathrm{TO}_1}(\nu)$ are undoubtedly different, as can be seen in Fig. 1. If the interaction between the Li-induced dipoles is based on the long-range Coulomb interaction, the temperature evolution of the host lattice polarizability should lead to modification of the interaction strength. We believe that close analysis of the extracted susceptibility combined with host lattice polarizability will produce new facts with regard to this system.

We have performed THz-TDS and dielectric spectroscopy below 1 MHz in $KTaO_3$ and KLT crystals from 6 to 300 K. Combining the data of THz-TDS with that obtained by dielectric spectroscopy below 1 MHz, we succeeded in separating the two dielectric origins, that is, the Li-induced quasistatic dipoles and the TO_1 soft mode. Temperature dependence of the complex dielectric constant purely originated from the Li-induced quasistatic dipoles is discussed in connection with LF-RP and HF-RP. The KLT crystals used in this study are of dilute Li concentrations $x=0.010$, 0.020, and 0.036 across the critical concentration $x_c \cong 0.022$,[15] since the situation becomes complicated for large Li concentrations because of the percolation of polar regions.[34] From the analysis of the dependence of the extracted susceptibility on host lattice polarizability, we concluded that two kinds of interaction should be relevant to the ordering of this system and the switch between the two should be responsible for whether the low-temperature phase becomes glassy or ferroelectric domain-state-like.[15]

II. EXPERIMENTAL

Pure $KTaO_3$ and KLT single crystals were grown by the spontaneous nucleation technique[51] using K_2CO_3, Li_2CO_3, and Ta_2O_5 powders as starting materials. The mixture was held in a 50 cc platinum crucible with a lid at 1450 °C for 2 h and cooled to room temperature with a cooling rate of 20 °C/h. As the flux, we placed the 47% mol concentration excess alkalis in the crucible. Single crystals with sizes of 1–10 mm were grown in the flux.

$$(1-x)K_2CO_3 + xLi_2CO_3 + Ta_2O_5 \rightarrow 2K_{1-x}Li_xTaO_3 + CO_2. \quad (2)$$

We denote KLT crystals made from different starting compositions of $x=0.010$, 0.020, and 0.040 as KLT1, KLT2, and KLT4, respectively, in this paper.

The starting composition x_m and the resultant composition x are generally different; thus, the resultant Li mol concentration of the grown crystals x was determined by comparing the experimental results of the crystals with that in the report by van der Klink *et al.*[12] For KLT2 and KLT4, we estimated the Li concentration according to the results of THz-TDS with field cooling using the relation $T_g = 535x^{0.66}$ K,[12] between the dipole freezing temperature T_g and the Li mol concentration x. The estimated Li concentrations were $x=0.020$ (KLT2) and 0.036 (KLT4). We regard 39 and 59 K, where the anisotropy of the phonon dielectric constant disappears in the zero-field heating process, as T_g for KLT2 and KLT4, respectively. The details of THz-TDS in field-cooled KLT will be presented in our next paper. For KLT1, in which such an anisotropy of the dielectric constant in the THz region was not observed by THz-TDS, we think of x in KLT1

as x_m=0.010. This seems satisfactory because the temperature dependence of the relaxation time of Li-induced dipoles is almost identical with that in KLT of x=0.011 in the report by van der Klink *et al.*[12]

The grown crystals were sliced into 50–60-μm-thick plates with a (001) cut surface and polished using a diamond slurry. The typical dimensions of the sample were about 7 $\times 7 \times 0.05$ mm^3. The sample thickness was determined by observing the cross sections using an optical microscope. We evaluated the thickness in the accuracy of 1 μm.

To evaluate the permittivity from 100 Hz to 1 MHz in the samples, ac impedance measurements were performed using an HP 4284A LCR meter with a probing field of 2 kV/m along [001]. The THz-TDS system was constructed using a mode-locked Ti: sapphire laser (Spectra-Physics, Tsunami, 70 fs pulse duration, 82 MHz repetition rate, and 810 nm center wavelength). The THz pulse was generated by optical rectification with a 2-mm-thick (110) ZnTe crystal[52] or by fs laser-irradiated (100) InAs in a 1 T magnetic field[53] and detected using the electro-optic (EO) sampling technique with a 1-mm-thick (110) ZnTe crystal.[54] The generated THz radiation was collimated and focused on the sample by two off-axis parabolic mirrors. The polarization of the THz wave was horizontally fixed in parallel to the [100] axis. A sample was mounted on a copper plate with a transmission hole having a diameter of 4 mm, through which the THz wave was transmitted. The copper plate was mounted on a copper cold finger whose temperature could be varied from 6 K to room temperature in a conductive-type liquid helium cryostat. The transmitted THz wave was collected and focused on the ZnTe crystal with two parabolic mirrors. The birefringence of the sampling beam induced by the EO effect with the electric field of the THz pulse was detected using a polarimeter.[54] For phase-sensitive detection, the fs laser beam for THz generation was modulated using an acousto-optic modulator operating at 80 kHz. The detectable spectral range in this system was from 0.3 THz to 2.5 THz with a sensitivity of $S/N \sim 1500$ in electric-field amplitude.

III. RESULTS

A. Temperature dependence of terahertz time-domain spectra

Figure 2(a) shows the waveforms of the THz pulses transmitted through the KLT2 crystal at 303, 99, 59, and 20 K. The temporal profile of the THz pulse without the sample is also presented at the top of Fig. 2(a). At 303 K, the insertion of the sample causes a 2.5 ps time delay of the maximum peak and reduces the electric field amplitude to about 1/10. These effects show that the sample has a large dielectric constant in the THz region. The refractive index in the THz region is estimated as $n \cong 15$ from the time delay and the thickness of the sample (52 μm). The following small pulse of around 8 ps is caused by internal reflections of the sample.[37] With decreasing temperature, the arrival of the transmitted pulse is dramatically delayed. This means that the index of the refraction in the THz region increases with decreasing temperature. In addition, the amplitude of the signal becomes weaker and weaker. The attenuation of the pulse means an enhancement of the reflection and/or absorption in the sample. These temperature dependences are attributed to softening of the TO_1 mode, which has been already reported in pure $KTaO_3$ crystal.[37]

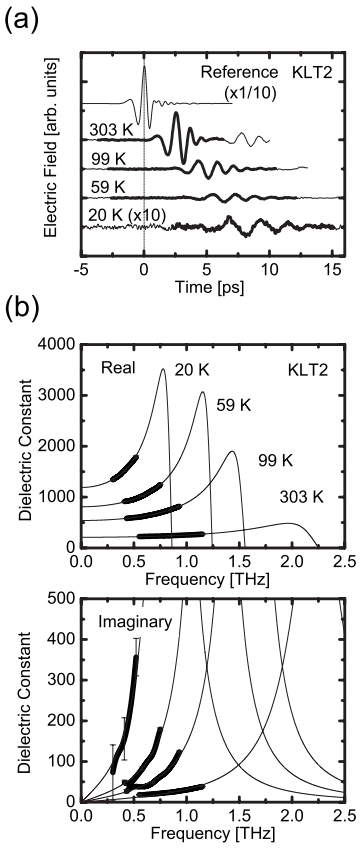

FIG. 2. (a) Waveforms of THz pulses transmitted through a $K_{1-x}Li_xTaO_3$ (x=0.020) single crystal with a 52 μm thickness at several temperatures. A temporal profile without a sample is presented over the transmitted spectra for the reference on a scale of 1/10. The first pulses without any internal reflections are drawn by thick curves. We used the first pulses for the derivation of the complex dielectric constant. (b) Frequency dispersion of the real part and the imaginary part of complex dielectric constants in a $K_{1-x}Li_xTaO_3$ (x=0.020) crystal at several temperatures. Bold curves are experimental results obtained by THz-TDS. Thin curves are dispersions reproduced by a single Lorentz oscillator model substituted by the best set of parameters.

We have derived the complex dielectric constant $\tilde{\epsilon}(\nu)$ directly from the Fourier component of transmitted waveforms in the time domain. In our derivation, the internal multireflection effect, which corresponds to the pulse sequence following the first pulse in Fig. 2(a), is ignored to avoid analytical complexity. The time regions used in our analysis at each temperature are indicated by thick curves in Fig. 2(a). In this case, the Fourier component at frequency ν of the transmitted electric field $\tilde{E}_t(\nu)$ and the reference electric field measured without a sample $\tilde{E}_{\mathrm{ref}}(\nu)$ can be expressed as in Eqs. (3) and (4), respectively,

$$\tilde{E}_t(\nu) = \tilde{E}_0(\nu)\tilde{t}_{vs}(\nu)\exp\left(i\frac{2\pi\nu d\sqrt{\tilde{\epsilon}(\nu)}}{c}\right)\tilde{t}_{sv}(\nu) \qquad (3)$$

and

$$\tilde{E}_{\mathrm{ref}}(\nu) = \tilde{E}_0(\nu)\exp\left(i\frac{2\pi\nu d}{c}\right) \tag{4}$$

with the Fresnel coefficient at the boundary from the vacuum to the sample $\tilde{t}_{vs}(\nu)=2/[\sqrt{\tilde{\epsilon}(\nu)}+1]$ and that from the sample to the vacuum $\tilde{t}_{sv}(\nu)=2\sqrt{\tilde{\epsilon}(\nu)}/[\sqrt{\tilde{\epsilon}(\nu)}+1]$ for normal incidence. $\tilde{E}_0(\nu)$ is the electric field of the incident pulse, d is the thickness of the sample, and c is the velocity of light in vacuum. $\tilde{\epsilon}(\nu)$ can be directly obtained from the experimental values of $\tilde{E}_t(\nu)$ and $\tilde{E}_{\mathrm{ref}}(\nu)$ without resorting to the Kramers-Kronig relation.

In Fig. 2(b), the frequency dispersions of the real and imaginary parts of complex dielectric constants $\tilde{\epsilon}(\nu)$ at several temperatures are shown by thick curves. Both the real and imaginary parts increase monotonically with frequency, and the increments become larger at lower temperatures. The observed dispersions are the low-energy shoulder of the TO_1-mode resonance.[34,37] The thin curves in Fig. 2(b) are the dielectric constants due to the TO_1 soft mode calculated by a single Lorentz oscillator model

$$\tilde{\epsilon}^{\mathrm{THz}}(\nu) = \tilde{\epsilon}_\infty + \tilde{\chi}_{\mathrm{TO}_1}(\nu) = \tilde{\epsilon}_\infty + \frac{(\epsilon_0^{\mathrm{THz}} - \tilde{\epsilon}_\infty)\nu_0^2}{\nu_0^2 - \nu^2 - i\nu\gamma_0}, \tag{5}$$

where ν_0, γ_0, $\epsilon_0^{\mathrm{THz}}$, and $\tilde{\epsilon}_\infty$ are the mode frequency, damping constant, and low- and high-frequency limits of the relative complex dielectric constant, respectively. In this analysis, the value of $\tilde{\epsilon}_\infty=13.8$ was used. According to the authors in Refs. 34 and 35, the two additional higher-energy infrared-active phonons have oscillator strengths of 6.3 and 2.5 in addition to the optic permittivity of 5.

Three parameters ν_0, γ_0, and $\epsilon_0^{\mathrm{THz}}$, were determined by performing a least-squares fit with Eq. (5) to the experimental data. Although we observed only the shoulder of the TO_1-mode resonance, simultaneous fitting for real and imaginary parts enabled us to successfully determine the dispersion of the TO_1 mode in the framework of the single Lorentz oscillator model. Drawing the contour surfaces of the mean square error, we ascertained that the best of $(\nu_0, \gamma_0, \epsilon_0^{\mathrm{THz}})$ is the only minimum in the 3D-parameter space. Among the three parameters, $\epsilon_0^{\mathrm{THz}}$ was the most accurately obtained, with accuracy of less than 5%. The dependence of the fitting results on $\tilde{\epsilon}_\infty$ was also checked by varying $\tilde{\epsilon}_\infty$ from 1 to 50. The obtained $\epsilon_0^{\mathrm{THz}}$ for $1\leq\tilde{\epsilon}_\infty\leq 50$ is in accordance with less than 1% error while the other two parameters showed ~10% errors.

B. THz-TDS in zero-field cooled KLT

Figure 3 shows the temperature dependence of the static dielectric constant from the fit to THz data. As the temperature decreases, the static dielectric constant increases in the KLT samples, showing saturation in the low-temperature region. The static dielectric constant due to the soft mode below 100 K decreases dramatically with increasing the Li concentration. A decrease in the soft-mode static dielectric constant means a high-frequency shift of the TO_1-mode frequency under fixed LO_1-mode frequency.[55] The TO_1-mode frequency is related to the static dielectric constant by the LST relation

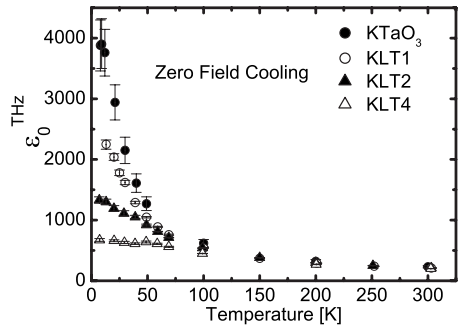

FIG. 3. Temperature dependence of the static dielectric constant in $K_{1-x}Li_xTaO_3$ crystals obtained from the fit to THz data for $x=0$ (closed circles), 0.010 (open circles), 0.020 (closed triangles), and 0.036 (open triangles).

$$\left(\frac{\nu_0^{\mathrm{TO}}}{\nu_0^{\mathrm{LO}}}\right)^2 = \frac{\tilde{\epsilon}_\infty}{\tilde{\epsilon}_0^{\mathrm{THz}}}, \tag{6}$$

where ν_0^{TO}, ν_0^{LO}, ϵ_0, and ϵ_∞ are the frequencies of the transverse and longitudinal optical phonons and the static and background dielectric constants, respectively. Stiffening of the TO_1 mode brought about by Li substitution was observed by hyper-Raman scattering,[31] neutron scattering,[30] and IR spectroscopy combined with THz-TDS.[34,35]

In Fig. 4, we present the static dielectric constant of the soft mode for KLT1 with the permittivities measured by the LCR meter at three frequencies. The permittivity obtained by the ac impedance measurement exhibits a broad frequency-dependent peak structure at around 50 K with strong frequency dispersion in all the KLT samples, unlike the data of THz-TDS, which exhibit a plateaulike behavior.[34–36] The peak temperature at 100 Hz is 45 K, and that at 1 MHz is 70 K. Throughout this paper, we define the peak temperature at 100 Hz as $T_m^{100\ \mathrm{Hz}}$. $T_m^{100\ \mathrm{Hz}}$ in KLT1, KLT2, and KLT4 is 45, 50, and 60 K, respectively. Such a strongly frequency-dependent broad peak is due to the dipolar glasslike response typical of relaxor materials.[3,4] The characteristic frequency of the relaxation mode in KLT1 is about 1 kHz at 45 K and 1 MHz at 66 K, which is consistent with the data in the study of van der Klink *et al.* on KLT with a similar Li

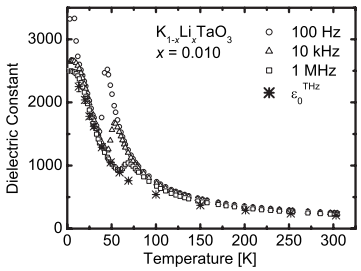

FIG. 4. Temperature dependence of the static dielectric constant determined by THz-TDS and permittivity measured at three frequencies in $K_{1-x}Li_xTaO_3$ crystals for $x=0.010$. The asterisks indicate the static dielectric constant determined by THz-TDS. The open circles, open triangles, and open squares show the permittivity measured by an LCR meter at 100 Hz, 10 kHz, and 1 MHz, respectively.

concentration.[12] The slowing relaxational mode is below 10 GHz below room temperature.[36] On the other hand, the static dielectric constant obtained by THz-TDS and the dielectric constants measured at frequencies lower than 1 MHz show similar temperature dependences below $T_m^{100\ \mathrm{Hz}}$. This fact indicates that the static dielectric constant in KLT below $T_m^{100\ \mathrm{Hz}}$ mainly originates from the TO_1 soft mode.[36]

As is described in the previous section, THz-TDS reveals a dielectric response due to the TO_1 soft mode. Therefore, the low-frequency limit (static limit) of $\tilde{\epsilon}^{\mathrm{THz}}(\nu)$ given by

$$\epsilon_0^{\mathrm{THz}} = \tilde{\chi}_{\mathrm{TO}_1}(0) + \epsilon_\infty, \tag{7}$$

corresponds to the high-frequency limit of the susceptibility, $\tilde{\chi}_{\mathrm{Li}}(\nu)$, since 10 GHz is almost static for the oscillator in the THz region. Equation (1) can be written as

$$\tilde{\epsilon}_r(\nu) = \tilde{\chi}_{\mathrm{Li}}(\nu) + \epsilon_0^{\mathrm{THz}} \tag{8}$$

for $\nu < 10$ GHz. The word "quasistatic" is used according to Vogt,[14] meaning that Li-induced dipoles are dynamic for observers below 10 GHz but static for those in the THz region since the frequency of the relaxation of Li-induced dipoles is, at most, in the order of 10 GHz.[36]

For an ideal Debye relaxation system, the complex dynamical susceptibility $\tilde{\chi}(\nu,T)$ is given by

$$\mathrm{Re}[\tilde{\chi}(\nu,T)] = \frac{\tilde{\chi}(0,T)}{1+(\nu\tau)^2} + \chi_{\mathrm{HF}} \tag{9}$$

and

$$\mathrm{Im}[\tilde{\chi}(\nu,T)] = \frac{\nu\tau\tilde{\chi}(0,T)}{1+(\nu\tau)^2}, \tag{10}$$

where $\tilde{\chi}(0,T)$, τ, χ_{HF}, and ν are the static susceptibility due to dipoles, the relaxation time, the susceptibility due to other dielectric origins in the high-frequency region, and the frequency of the ac field, respectively. Since the imaginary part of $\tilde{\chi}(\nu,T)$ is almost zero and the real part is almost constant at 100 Hz in the frequency region, $\tilde{\chi}(100\ \mathrm{Hz},T)$ can be used as the static limit of $\tilde{\chi}(\nu,T)$, that is, $\tilde{\chi}(0,T)$. This is because the condition $\nu \ll \tau^{-1}$ is satisfied at 100 Hz for the KLT system except at temperatures around $T_m^{100\ \mathrm{Hz}}$ and 100 K,[36] as will be reported later.

In all the samples,

$$\tilde{\chi}_{\mathrm{Li}}(100\ \mathrm{Hz}) = \tilde{\epsilon}_r(100\ \mathrm{Hz}) - \epsilon_0^{\mathrm{THz}} \tag{11}$$

takes a finite value even at room temperature.[34–36] This means that the static susceptibility due to Li-induced quasistatic dipoles is separable from that of the TO_1 soft mode even at room temperature.

Figure 5(a) shows the temperature dependence of the real part of $\tilde{\chi}_{\mathrm{Li}}(100\ \mathrm{Hz})$, denoted by $\chi_{\mathrm{Li}}(T)$, in KLT1 and KLT4. $\chi_{\mathrm{Li}}(T)$ increases monotonically with decreasing temperature and takes the maximum at $T_m^{100\ \mathrm{Hz}}$. The reciprocal susceptibility at 100 Hz, $\chi_{\mathrm{Li}}(T)^{-1}$, is shown in Fig. 5(b). Remarkably, $\chi_{\mathrm{Li}}(T)^{-1}$ in KLT1 exhibits a linear temperature dependence from 300 to 100 K, obeying a simple Curie-Weiss law with $T_c = 50$ K. Below 100 K, it deviates from the Curie-Weiss line. On the other hand, $\chi_{\mathrm{Li}}(T)^{-1}$ in KLT4 shows a concave curve with decreasing temperature above 100 K rather than a linear temperature dependence.

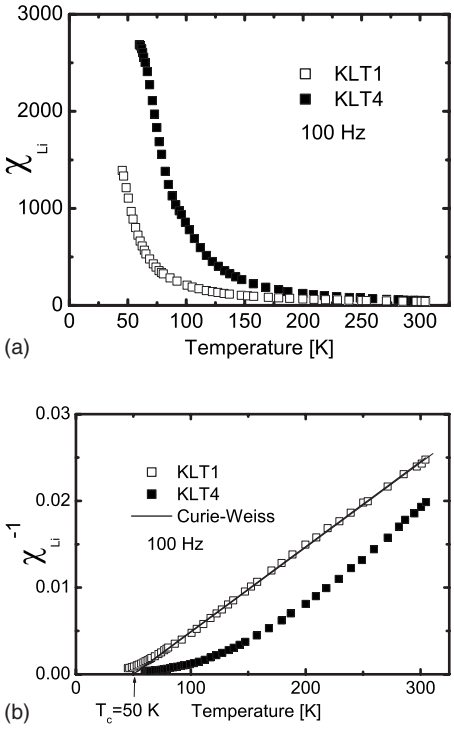

FIG. 5. Temperature dependences of (a) the susceptibility at 100 Hz due to Li-induced dipoles in $K_{1-x}Li_xTaO_3$ crystals for $x = 0.010$ (KLT1) and 0.036 (KLT4) and (b) those of the reciprocal susceptibility at 100 Hz. The susceptibility is obtained by subtracting $\epsilon_0^{\mathrm{THz}}$ from $\tilde{\epsilon}_r(100\ \mathrm{Hz})$. Open squares and closed squares are the data on KLT1 and KLT4, respectively. (b) The solid line indicates the Curie-Weiss law derived from the data of KLT1 above 100 K. The Curie temperature is 50 K.

IV. DISCUSSION

A. Anomaly in the susceptibility of Li-induced polarizations

To clarify the influence of the lattice polarizability on interacting Li-induced dipoles, we analyze the temperature dependence of $\chi_{\mathrm{Li}}(T)^{-1}$. Generally, when ferroelectric ordering is driven by a temperature-independent interaction, the permittivity obeys a Curie-Weiss law with a constant Curie-Weiss temperature as required by the mean-field theory. However, in this system, whose background permittivity due to the host lattice, i.e., $\epsilon_0^{\mathrm{THz}}$, changes with the temperature, the interaction between the Li-induced dipoles should be changed, causing the evolution of the Curie-Weiss temperature. To visualize this effect, the Curie-Weiss temperature at each temperature must be given. Therefore, we deduce experimentally the temperature dependence of the tangential line of $\chi_{\mathrm{Li}}(T)^{-1}$, defined as

$$y = \alpha(T)[T - T_0(T)] \tag{12}$$

with

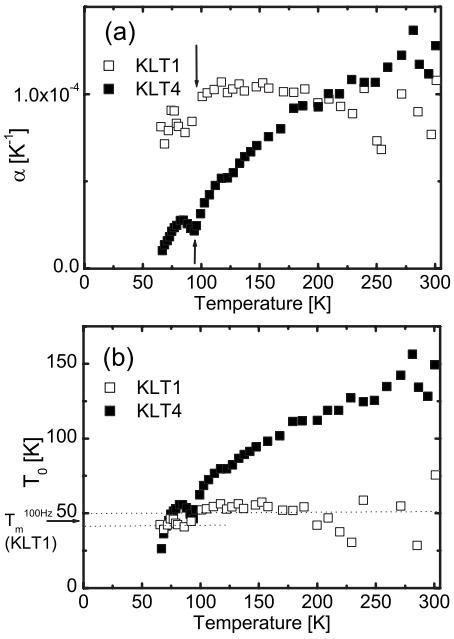

FIG. 6. Temperature dependences of (a) the slope and (b) the crossing point with the horizontal axis of the tangential lines on the reciprocal static dielectric constant due to Li-induced dipoles in the $K_{1-x}Li_xTaO_3$ crystals for $x=0.010$ (KLT1) and 0.036 (KLT4). The open squares and closed squares are the data on KLT1 and KLT4, respectively. (a) The temperature, denoted as T_a in context, for the susceptibility to change the temperature dependence is represented by arrows. (b) The horizontal dotted lines show Curie temperatures in KLT1 above and below T_a. The arrow indicates the peak temperature of the permittivity in KLT1 measured at 100 Hz.

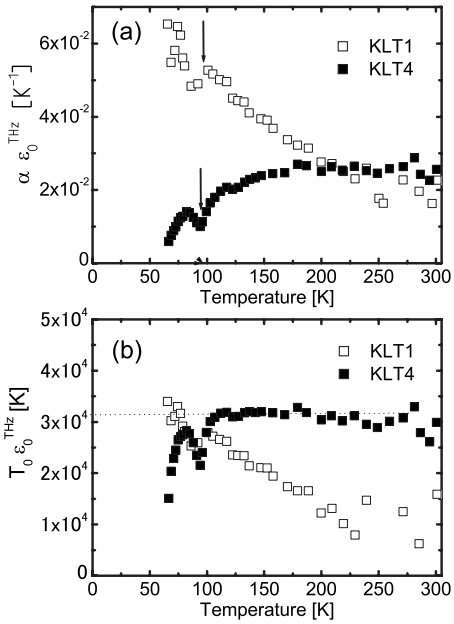

FIG. 7. Temperature dependences of (a) the slope and (b) the crossing point with the horizontal axis multiplied by the static dielectric constant obtained by THz-TDS in the $K_{1-x}Li_xTaO_3$ crystals with $x=0.010$ (KLT1) and 0.036 (KLT4). The temperature dependences of the slope and the crossing point with the horizontal axis were obtained from the tangential lines on the reciprocal static dielectric constant due to Li-induced dipoles. The temperature dependence of the static dielectric constant of the host lattice $\epsilon_0^{\mathrm{THz}}(T)$ was determined by THz-TDS. (a) The arrows indicate the temperature of the anomaly in the susceptibility. (b) The horizontal dotted lines show typical values of the products above T_a in KLT4.

$$\alpha(T) = \frac{\partial[\chi_{\mathrm{Li}}(T)^{-1}]}{\partial T} \tag{13}$$

and

$$T_0(T) = T - \frac{\chi_{\mathrm{Li}}(T)^{-1}}{\alpha(T)}. \tag{14}$$

If a system obeys an ideal Curie-Weiss law, $\alpha(T)$ and $T_0(T)$ are unchanged and $T_0(T)$ corresponds to the Curie-Weiss temperature. In Figs. 6(a) and 6(b), we show the temperature dependences of $\alpha(T)$ and $T_0(T)$, which are determined numerically using the three adjacent bits of data shown in Fig. 5(b).

In Figs. 6(a) and 6(b), anomalies in $\alpha(T)$ and $T_0(T)$ can be seen at around 100 K in both KLT1 and KLT4. Obviously, $\alpha(T)$ and $T_0(T)$ change their temperature dependences across the temperature. We denote the temperature as T_a, at which the anomaly appears as shown in Figs. 6(a) and 7(a). T_a in KLT1, KLT2, and KLT4 is 96 ± 4 K, 95 ± 4 K, and 93 ± 2 K, respectively. The appearance of T_a is attributed to the critical slowing down of LF-RP. As Bovtun *et al.* reported, the lowering relaxation frequency of LF-RP goes across 100 Hz at around 100 K.[36] The fact that T_a is hardly changed by the Li concentration also supports this assignment because the temperature dependence of the relaxation frequency of LF-RP is almost identical independently of the Li concentration.[12] Below T_a, the relaxation frequency of LF-RP slows down to the order of mHz at 70 K.[12] Relevant deformations associated with LF-RP in the extremely long relaxation time should perturb the susceptibility due to the faster HF-RP, leading to the steplike change in the temperature dependence. However, the dielectric contribution of LF-RP is so small even in KLT4, considering that the sizes of dielectric steps of LF-RP and HF-RP for $x<0.04$,[45] that most part of the extracted susceptibility can be regarded as that of HF-RP. Only around the critical temperature (100 K), LF-RP gives finite contributions as dip structures. In the following section, we will discuss the property of the interaction related to HF-RP.

B. Ordering of the Li-induced polarizations

In KLT1, $\alpha(T)$ and $T_0(T)$ are almost constant above T_a, indicating the Curie-Weiss behavior above T_a. $\chi_{\mathrm{Li}}(T)$ obeys a simple Curie-Weiss law regardless of whether the permittivity of the host lattice is enhanced at low temperatures. This is an unexpected behavior considering the property of the interaction, whose origin has been attributed to the long-range Coulomb interaction. If the interaction between the Li-induced dipoles originates from the electrostatic Coulomb interaction, the interaction must be weakened by the increasing permittivity due to the host lattice by the factor of $\epsilon_0^{\mathrm{THz}}(T)^{-1}$. The upper dotted line in Fig. 6(b) represents the

Curie-Weiss temperature $T_c=50$ K in the high-temperature region. Across T_a, $\alpha(T)$, and $T_0(T)$ in KLT1 show a steplike change. The lower dotted line in Fig. 6(b) represents a Curie-Weiss temperature below 92 K. The second Curie-Weiss temperature $T_c'=43$ K seems to coincide with $T_m^{100\ \mathrm{Hz}}$.

In contrast, $\alpha(T)$ and $T_0(T)$ in KLT4 decrease monotonically with lowering temperature above 103 K. The situation in KLT4 is quite different from that observed in KLT1. The monotonic decrease of $T_0(T)$ with decreasing temperature suggests a screening effect of $\epsilon_0^{\mathrm{THz}}(T)$ on the interaction. Assuming that the interaction originates from the long-range electrostatic Coulomb interaction, the Curie temperature, which should be proportional to the interaction, must show a similar temperature evolution to $\epsilon_0^{\mathrm{THz}}(T)^{-1}$.

Figures 7(a) and 7(b) show the temperature dependences of $\alpha(T)$ and $T_0(T)$, which are multiplied by $\epsilon_0^{\mathrm{THz}}(T)$. As expected, $\alpha(T)\epsilon_0^{\mathrm{THz}}(T)$ and $T_0(T)\epsilon_0^{\mathrm{THz}}(T)$ in KLT4 are almost independent of the temperature above T_a, meaning that $\alpha(T)\propto\epsilon_0^{\mathrm{THz}}(T)^{-1}$ and $T_0(T)\propto\epsilon_0^{\mathrm{THz}}(T)^{-1}$ are above T_a. This result suggests that the dominant interaction in KLT4 above T_a should be the long-range Coulomb interaction. It is noteworthy that $\chi_{\mathrm{Li}}(T)$ in KLT1 obeys a Curie-Weiss law by itself, while that multiplied by $\epsilon_0^{\mathrm{THz}}(T)$ largely deviates from a Curie-Weiss law.

The results are summarized as follows: (i) In KLT1, which corresponds to $x<x_c$, $\chi_{\mathrm{Li}}(T)$ obeys a simple Curie-Weiss law above T_a. (ii) In KLT4, which corresponds to $x>x_c$, $\chi_{\mathrm{Li}}(T)$ obeys a modified Curie-Weiss law whose Curie-Weiss temperature is inversely proportional to $\epsilon_0^{\mathrm{THz}}(T)$ above T_a. (iii) In KLT1, $\chi_{\mathrm{Li}}(T)$ below T_a shows a second Curie-Weiss behavior with reduced Curie temperature that is similar to $T_m^{100\ \mathrm{Hz}}$.

As described in the Introduction, it is well established that $T_m^{100\ \mathrm{Hz}}$ corresponds to the temperature for the motion of $\pi/2$-flipping Li ions to freeze. From results (i) and (iii), we attribute the origin of the observed Curie-Weiss law in $\chi_{\mathrm{Li}}(T)$ to the HF-RP. The shift of the Curie-Weiss temperature at T_a should be caused by relevant lattice deformations or displacements involved in LF-RP with the lengthened relaxation time. The positive Curie-Weiss temperature also suggests the existence of relevant interaction that drives the $\pi/2$ flipping Li-induced dipoles to order. This interaction, denoted as $J_{\mathrm{Li\text{-}Li}}$, is almost constant and independent of the temperature evolution of the host lattice polarizability. This never seems to be predictable for the traditional theories on relaxor material based on the Coulomb interaction.[1,3,4,56–58]

On the other hand, from result (ii), the dominant interaction for $x>x_c$ should be the Coulomb interaction, denoted as J_{C}, because of the inversely proportional dependence of the Curie temperature on $\epsilon_0^{\mathrm{THz}}$. Considering that J_{C} is screened by $\epsilon_0^{\mathrm{THz}}(T)$, we attribute the origin of J_{C} to the long-range electrostatic Coulomb interaction as expressed by

$$J_{\mathrm{C}}\propto\epsilon_0^{\mathrm{THz}}(T)^{-1}r^{-2}\propto\epsilon_0^{\mathrm{THz}}(T)^{-1}x^{2/3}, \tag{15}$$

where r is the average of the distance between the nearest neighbor dipoles. This qualitatively explains the increase of J_{C} with increasing the Li concentration x.

The temperature dependence of $\chi_{\mathrm{Li}}(T)$ due to HF-RP above T_a is essentially different in two cases of $x<x_c$ and $x>x_c$. The dominant interaction, which governs $\chi_{\mathrm{Li}}(T)$ due to HF-RP above T_a, should be changed when the concentration x exceeds the critical density x_c. The boundary between the glasslike phase ($x<x_c$) and the ferroelectric domain-state-like phase ($x>x_c$) (Refs. 15 and 27) may be determined by the competition between the two interactions: when the Li concentration is smaller than x_c, J_{C} hardly works, and only $J_{\mathrm{Li\text{-}Li}}$ becomes dominant, causing the system to be glassy without a long-range correlation.[15,27] When the Li concentration is larger than x_c, J_{C} becomes dominant above T_a and forms a long-range correlation, leading to the low-temperature ferroelectric domain-state-like phase.[15,27] Considering that $J_{\mathrm{Li\text{-}Li}}$ is hardly influenced by the evolution of the host lattice polarizability, $J_{\mathrm{Li\text{-}Li}}$ should be a short-range interaction that cannot form a long-range ferroelectric order by itself. Plausible candidates for $J_{\mathrm{Li\text{-}Li}}$ are an elastic coupling between Li ions[59–61] or, perhaps, a coupling assisted by a phonon in the Brillouin zone boundary.[29,62]

As for the origin of LF-RP, the most recent results by Yokota *et al.* seem to provide significant information on LF-RP. They determined Burn's temperature[63] T_B, where the formations of polar clusters begin to take place, by their optical second harmonic generation observations and x-ray diffraction experiments in 3%-KLT and 7%-KLT, and found that the Burn's temperature of about 90 K in their 3%-KLT sample is at least 30 K higher than the $T_m^{100\ \mathrm{Hz}}$.[16] T_B in their 3%-KLT sample whose $T_m^{100\ \mathrm{Hz}}$ lies between those of KLT2 and KLT4 is remarkably close to the nearly constant T_a for $0.010\leq x\leq 0.036$. This suggests that the observed T_a corresponds to the T_B and that the formations of polar clusters begin with the critical slowdown of LF-RP for $0.010\leq x\leq 0.036$. In addition, the reported "tetragonal weak lattice deformation"[16] seems to strongly link to the freezing motion of LF-RP. Considering the absence of SH intensity, which is sensitive to a breaking of the inversion symmetry, at T_B in 3%-KLT and quite a small dielectric step of LF-RP for $x<0.04$,[45] the freezing motion of LF-RP for $0.010\leq x\leq 0.036$ appears to be a nonpolar motion which keeps the polar HF-RP from forming clusters. Although we have no idea about why their 7%-KLT is not the case, it is quite interesting that the temperature dependence of the "tetragonality" in 7%-KLT has an inflection point at around T_a and that the rise of the SH intensity in 7%-KLT is suppressed above T_a.

V. CONCLUSION

We have succeeded in extracting the dielectric susceptibility purely originated from the Li-induced quasistatic dipoles in relaxor KLT from 300 K to the dipole freezing temperature by terahertz time-domain spectroscopy. The extracted susceptibility and its temperature dependence change with the critical slowdown of the low-frequency relaxation process in KLT. The extraction of the susceptibility also

revealed that the dominant interaction that drives the high-frequency relaxation process is essentially different above T_a across the critical concentration x_c. The crossover from the low-temperature glasslike phase to the low-temperature ferroelectric domain state across x_c is attributed to the interplay of the two kinds of interaction. For $x<x_c$, a short-range interaction between individual $\pi/2$-flipping Li ions, which is impervious to the polarizability of the host lattice and is responsible for the dipole freezing, becomes dominant. For $x>x_c$, the interaction originated from the long-range electrostatic Coulomb interaction, which is screened by the polarizability of the host lattice, becomes dominant over the short-range interaction.

ACKNOWLEDGMENTS

The authors thank M. Shirai for his participation in very fruitful discussions. This work was supported by the SCOPE program (Grant No. 032207004) from the Ministry of Public Management, Home Affairs, Posts, and Telecommunications, Japan. The authors also acknowledge a grant-in-aid for the 21st Century COE "Center for Diversity and Universality in Physics" and Scientific Research on Priority Areas, and for the Creative Scientific Research program (Grant No. 18GS0208) from the Ministry of Education, Culture, Sports, Science, and Technology (MEXT) of Japan.

*kochan@scphys.kyoto-u.ac.jp

[1] B. E. Vugmeister and M. D. Glinchuk, Rev. Mod. Phys. **62**, 993 (1990).
[2] U. T. Höchli, K. Knorr, and A. Loidl, Adv. Phys. **39**, 405 (1990); **51**, 589 (2002).
[3] G. A. Samara, in *Solid State Physics*, edited by H. Ehrenreich and F. Spaepen (Academic Press, New York, 2001), Vol. 56, p. 239–458.
[4] G. A. Samara, J. Phys.: Condens. Matter **15**, R367 (2003).
[5] J. H. Barrett, Phys. Rev. **86**, 118 (1952).
[6] J. J. van der Klink and F. Borsa, Phys. Rev. B **30**, 52 (1984).
[7] J. J. van der Klink and S. N. Khanna, Phys. Rev. B **29**, 2415 (1984).
[8] Y. Yacoby and A. Linz, Phys. Rev. B **9**, 2723 (1974).
[9] Y. Yacoby and S. Just, Solid State Commun. **15**, 715 (1974).
[10] F. Borsa, U. T. Höchli, J. J. van der Klink, and D. Rytz, Phys. Rev. Lett. **45**, 1884 (1980).
[11] U. T. Höchli, Phys. Rev. Lett. **48**, 1494 (1982).
[12] J. J. van der Klink, D. Rytz, F. Borsa, and U. T. Höchli, Phys. Rev. B **27**, 89 (1983).
[13] H. Vogt, Ferroelectrics **184**, 31 (1996).
[14] H. Vogt, Ferroelectrics **202**, 157 (1997).
[15] W. Kleemann, S. Kütz, and D. Rytz, Europhys. Lett. **4**, 239 (1987).
[16] H. Yokota, Y. Uesu, C. Malibert, and J. M. Kiat, Phys. Rev. B **75**, 184113 (2007).
[17] P. Doussineau, Y. Farssi, C. Frénois, A. Levelut, K. McEnaney, J. Toulouse, and S. Ziolkiewicz, Phys. Rev. Lett. **70**, 96 (1993).
[18] J. Toulouse, B. E. Vugmeister, and R. Pattnaik, Phys. Rev. Lett. **73**, 3467 (1994).
[19] R. K. Pattnaik and J. Toulouse, Phys. Rev. B **60**, 7091 (1999).
[20] R. K. Pattnaik, J. Toulouse, and B. George, Phys. Rev. B **62**, 12820 (2000).
[21] S. A. Prosandeev, V. A. Trepakov, M. E. Savinov, L. Jastrabik, and S. E. Kapphan, J. Phys.: Condens. Matter **13**, 719 (2001).
[22] S. A. Prosandeev, V. A. Trepakov, M. E. Savinov, and S. E. Kapphan, J. Phys.: Condens. Matter **13**, 9749 (2001).
[23] P. DiAntonio, B. E. Vugmeister, J. Toulouse, and L. A. Boatner, Phys. Rev. B **47**, 5629 (1993).
[24] M. Maglione, S. Rod, and U. T. Höchli, Europhys. Lett. **4**, 631 (1987).
[25] G. A. Azzini, G. P. Banfi, E. Giulotto, and U. T. Höchli, Phys. Rev. B **43**, 7473 (1991).
[26] P. Voigt and S. Kapphan, J. Phys. Chem. Solids **55**, 853 (1994).
[27] S. R. Andrews, J. Phys. C **18**, 1357 (1985).
[28] G. Yong, J. Toulouse, R. Erwin, S. M. Shapiro, and B. Hennion, Phys. Rev. B **62**, 14736 (2000).
[29] R. L. Prater, L. L. Chase, and L. A. Boatner, Phys. Rev. B **23**, 5904 (1981).
[30] W. A. Kamitakahara, C.-K. Loong, G. E. Ostrowski, and L. A. Boatner, Phys. Rev. B **35**, 223 (1987).
[31] H. Vogt, J. Phys.: Condens. Matter **7**, 5913 (1995).
[32] M. C. Nuss and J. Orenstein, in *Millimeter and Submillimeter Wave Spectroscopy of Solids*, edited by G. Grüner (Springer-Verlag, Berlin, 1998), p. 7.
[33] D. H. Auston, Appl. Phys. Lett. **43**, 713 (1983).
[34] V. Železný, A. Pashkin, J. Petzelt, M. Savinov, V. Trepakov, and S. Kapphan, Ferroelectrics **302**, 195 (2004).
[35] J. Petzelt, S. Kamba, V. Bovtun, and A. Pashkin, Ferroelectrics **298**, 219 (2004).
[36] V. Bovtun, V. Porokhonskyy, M. Savinov, A. Pashkin, V. Zelezny, and J. Petzelt, J. Eur. Ceram. Soc. **24**, 1545 (2004).
[37] Y. Ichikawa, M. Nagai, and K. Tanaka, Phys. Rev. B **71**, 092106 (2005).
[38] A. Pashkin, V. Železný, and J. Petzelt, J. Phys.: Condens. Matter **17**, L265 (2005).
[39] P. Mounaix, M. Tondusson, L. Sarger, D. Michau, V. Reymond, and M. Maglione, Jpn. J. Appl. Phys. **44**, 5058 (2005).
[40] J. Macutkevic, S. Kamba, J. Banys, A. Brilingas, A. Pashkin, J. Petzelt, K. Bormanis, and A. Sternberg, Phys. Rev. B **74**, 104106 (2006).
[41] J. Hlinka, J. Petzelt, S. Kamba, D. Noujni, and T. Ostapchuk, Phase Transit. **79**, 41 (2006).
[42] U. T. Höchli and M. Maglione, J. Phys.: Condens. Matter **1**, 2241 (1989).
[43] U. T. Höchli, J. Hessinger, and K. Knorr, J. Phys.: Condens. Matter **3**, 8377 (1991).
[44] P. Doussineau, Y. Farssi, C. Frénois, A. Levelut, K. McEnaney, J. Toulouse, and S. Ziolkiewicz, Europhys. Lett. **21**, 323 (1993).
[45] U. T. Höchli and D. Baeriswyl, J. Phys. C **17**, 311 (1984).
[46] H. M. Christen, U. T. Höchli, A. Chatelâin, and S. Ziolkiewicz, J. Phys.: Condens. Matter **3**, 8387 (1991).
[47] P. Doussineau, C. Frénois, U. T. Höchli, A. Levelut, and S. Ziolkiewicz, Ferroelectrics **127**, 241 (1992).

[48] Y. M. Poplavko, V. P. Bovtun, and I. N. Geifman, Izv. Akad. Nauk. SSSR, Fiz. Zemli **47**, 648 (1983).
[49] V. P. Bovtun, P. P. Syrnikov, N. K. Yushin, and Y. M. Poplavko, Izv. Akad. Nauk. SSSR, Fiz. Zemli **49**, 293 (1985).
[50] B. E. Vugmeister and M. D. Glinchuk, Sov. Phys. JETP **52**, 482 (1980).
[51] D. M. Hannon, Phys. Rev. **164**, 366 (1967).
[52] A. Rice, Y. Jin, X. F. Ma, X.-C. Zhang, D. Bliss, J. Larkin, and M. Alexander, Appl. Phys. Lett. **64**, 1324 (1994).
[53] N. Sarukura, H. Ohtake, S. Izumida, and Z. Liu, J. Appl. Phys. **84**, 654 (1998).
[54] Z. G. Lu, P. Campbell, and X.-C. Zhang, Appl. Phys. Lett. **71**, 593 (1997).
[55] C. H. Perry and N. E. Tornberg, Phys. Rev. **183**, 595 (1969).
[56] A. T. Fiory, Phys. Rev. B **4**, 614 (1971).
[57] G. D. Mahan, Phys. Rev. **153**, 983 (1967).
[58] G. D. Mahan and R. M. Mazo, Phys. Rev. **175**, 1191 (1968).
[59] U. T. Höchli, H. E. Weibel, and W. Rehwald, J. Phys. C **15**, 6129 (1982).
[60] A. S. Nowick and W. R. Heller, Adv. Phys. **12**, 251 (1963).
[61] K. Kaszyńska, Z. Trybula, M. D. Glinchuk, I. P. Bykov, and V. V. Laguta, Acta Phys. Pol. A **108**, 379 (2005).
[62] E. Courtens, J. Phys. C **14**, L37 (1981).
[63] G. Burns and F. H. Dacol, Solid State Commun. **48**, 853 (1983).